Flow cytometry and machine learning enable identification of allergenic urban tree pollen.

Authors : Sarah Tardif[1,2], Maria Raquel Kanieski[4], Gauthier Lapa[1,2], Grégoire Bonnamour[1,3], Rita Sousa-Silva[5], Isabelle Laforest-Lapointe[2,6], Alain Paquette[1,2]

[1] Département des sciences biologiques, Université du Québec à Montréal, Montréal, QC, Canada.
[2] Centre for Forest Research, Université du Québec à Montréal, Montréal, QC, Canada.
[3]Centre d'excellence en recherche sur les maladies orphelines-Fondation Courtois (CERMO-FC), Université du Québec à Montréal, Montréal, QC, Canada.
[4] Universidade do Estado de Santa Catarina, Depto. Engenharia Florestal, Lages, SC, Brasil.
[5] Institute of Environmental Sciences, Department of Environmental Biology, Leiden University, Leiden, The Netherlands.
[6] Département de Biologie, Université de Sherbrooke, Sherbrooke, QC, Canada.

Correspondence to: Sarah Tardif (sarahtardif02@gmail.com)

Abstract

Exposure to allergenic pollen is a major public health concern, as it is a key trigger for respiratory allergies, including seasonal allergic rhinitis, which affects approximately 20% of the global population. Monitoring airborne pollen is essential for prevention and clinical management, yet traditional identification methods, such as light microscopy, are time-consuming and often limited to genus- or family-level resolution. Here, we present a high-throughput approach combining flow cytometry with machine learning to identify pollen from urban environments. We collected a reference database of pollen from 97 species across 34 genera, representing the dominant allergenic trees and other common airborne taxa in Montreal, Canada. Using flow cytometry, we measured particle size, granularity, and fluorescence intensity across multiple excitation and emission channels, and applied a Random Forest classifier to distinguish pollen taxa. At the species level, the model achieved a mean F_1-score of 0.76, while genus-level classification reached 0.90, with misclassifications largely occurring among closely related species. Granularity and fluorescence parameters from the violet and blue lasers were the most distinctive features. Our results demonstrate that flow cytometry combined with machine learning provides an efficient, scalable alternative to microscopy, with potential for large-scale urban pollen monitoring.

1 Introduction

Exposure to allergenic pollen is a major public health concern, as it is a key risk factor for respiratory allergies. Seasonal allergic rhinitis affects approximately 20 % of the global population (Savouré et al., 2022) and is expected to worsen with climate change, which is projected to lengthen pollen seasons (Anderegg et al., 2021; Mousavi et al., 2024; Zhang and Steiner, 2022; Ziska et al., 2019). Rising temperatures and CO_2 levels stimulate plant growth, increasing pollen levels (Kim et al., 2018; Ladeau and Clark, 2006) and the allergenicity of pollen grains (Ahlholm et al., 1998; Kim et al., 2018). For allergy sufferers and healthcare providers, reliable pollen information, including which plant species and pollen traits contribute to different allergenicity properties, is essential for prevention and effective treatment, but remains scarce (Dunker et al., 2022; Medek et al., 2025; Sousa-Silva et al., 2020).

Expanding pollen monitoring networks in urban areas, which host most of the world's population, is increasingly recognized as essential (Tummon et al., 2024), yet this also requires processing a large number of pollen samples and thus highlights a clear need for efficient, ~~and~~ accurate, and high temporal resolution identification methods. Over the past decades, several analytical techniques have been developed for pollen detection and classification, each having advantages and limitations. Light microscopy remains the standard method used worldwide for pollen identification, but it is time-consuming and requires highly trained specialists (Brennan et al., 2019; Dunker et al., 2021, 2022; Gierlicka et al., 2022; de Weger et al., 2013). Although pollen morphology, defined by size, shape, apertures, and texture (Ogden et al., 1974; Smith, 1984), supports taxonomic identification, subtle interspecific differences restrict identification to genus or family level in most cases. Automated slide scanning, sometimes coupled with a machine learning algorithm, has improved efficiency but still faces limitations in distinguishing species from the same genus or family (Dunker et al., 2021; Holt and Bennett, 2014). Advanced imaging techniques, such as scanning electron microscopy (SEM), transmission electron microscopy (TEM), and optical diffraction tomography (ODT), provide much higher resolution for detailed analysis of pollen structures, but are costly or impractical for large-scale monitoring (Gierlicka et al., 2022). Molecular biology techniques, particularly metabarcoding and PCR-based methods, have the potential to enable species-level identification yet face challenges such as high costs, the presence of DNA inhibitors that can limit sensitivity and cause false negative, the limitations of taxonomic resolution, and the inability to quantify pollen abundance (Dunker et al., 2021; Gierlicka et al., 2022).

More recently, fluorescence spectroscopy and flow cytometry have emerged as promising approaches (Gierlicka et al., 2022; Šaulienė et al., 2019). These methods are based on the size and autofluorescence properties of particles, such as the pollen grains, and when combined with holographic images and machine

or deep learning, they can improve classification accuracy and enable automated (Dunker et al., 2022; Erb et al., 2024; Sikoparija et al., 2024; Swanson et al., 2023) and high-throughput identification (≈5000 grains s^{-1}) (Dunker et al., 2021; Gierlicka et al., 2022). Because each species has a specific fluorescence and granularity signature, it is possible to distinguish even morphologically similar taxa (Dunker et al., 2021).

Our study aims to develop a classification model capable of identifying pollen from urban environments at species and genus levels. Here we present the necessary first step in the development of a broader methodological pipeline for the analysis of airborne pollen ~~in urban environments~~. We built a reference collection representing the main tree species found across the city of Montreal, Canada. Unlike previous studies that rely on microscopic or imaging data, our approach relies exclusively on flow cytometry measurements, i.e. fluorescence intensity, particle size, and granularity to characterize pollen. This choice is motivated by the fact that most cytometers routinely used in healthcare and clinical settings are limited to these parameters. Consequently, developing a model based on these features enhances its applicability and ensures compatibility with the most widely implemented cytometry platforms. We then evaluated the performance of the machine-learning classification model trained on these flow cytometry parameters and identified those that contribute most to differentiating pollen species and genera.

2 Methodology

2.1 Pollen collection

To train the machine learning classification model, we created a reference database of pollen grains collected directly from plants of known species (mostly trees). The reference collection included pollen from both common urban tree species as well as widely planted hybrid cultivars.

Tree species were selected based on three criteria: (1) their relative abundance on the Island of Montreal, ensuring representation of the dominant urban taxa; (2) their anemophilous nature, since wind-pollinated species are typically the most allergenic (D'Amato et al., 2007; Falagiani, 1989); and (3) the inclusion of multiple species within each genus, to enable species-level discrimination where possible. Other species such as from the Rosaceae family were also included to increase resolution. For each selected species, pollen was collected from three individual trees from the Montreal Botanical Garden (for ease of identification) or among public trees across the city. At flowering time, ten floral units (flowers, catkins or male cones) were collected per tree, sampling different parts of the crown to capture intra-individual variation among pollen grains. We also included pollen from the Poaceae family (grasses) and the genus *Ambrosia* (ragweed), given their well-known allergenic potential (D'Amato et al., 2007; Falagiani, 1989). Their inclusion enabled the model to learn to discriminate tree pollen from other common airborne particle types, as real-world

environmental samples typically comprise a heterogeneous mix of tree, grass, and weed pollen, along with various non-pollen particulates. In the laboratory, floral units were placed in pre-labelled paper bags with desiccant gel. Pollen was extracted from the floral units using a filtration system that retained only particles between 5 and 100 µm in diameter, a size range that includes pollen grains but also particles of similar size. Filtration also prevents clogging of the flow cytometer because, as is generally recommended, particles should not exceed one-third to one-fifth of the width of the flow cell, which limits particle size to approximately 100 µm on the CytoFLEX instrument we used. The filtrate was then suspended in Dulbecco's phosphate-buffered saline (PBS) solution, a standard neutral isotonic buffer commonly used in flow cytometry to minimize aggregation (Aloisi et al., 2015; Dunker et al., 2021b) (see detailed protocol in the supplementary material). A subsample was examined under a light microscope to confirm the presence of pollen grains. If pollen was present, the sample was retained; if not, sampling was repeated, including filtration, and if necessary, additional flowers were collected.

2.2 Flow cytometry

Each pollen sample was analysed using flow cytometry (Fig. 1). Measurements were performed with a CytoFLEX cytometer (Beckam Coulter, Inc.), equipped with three excitation lasers at wavelengths of 405 nm (violet), 488 nm (blue), and 640 nm (red). Due to a hydrodynamic flow stream, each pollen grain passes sequentially through each laser, which excites fluorescent phenolic compounds present in the sporopollenin ~~the fluorescent proteins on the surface~~ of the pollen grain's outer wall. Depending on their peptide composition, these ~~proteins~~fluorophores absorb light at a certain wavelength and emit light radiation at a different wavelength in return producing a characteristic fluorescence signature that varies among species. For each laser, avalanche photodiode (APD) detectors measure the intensity of light emitted at different wavelengths using ten filters: 450/45, 525/40, 610/20 (violet laser), 525/40, 585/42, 690/50, 780/60 (blue laser), 660/10, 712/25, 780/60 nm (red laser). Each filter value, such as 450/45, follows a simple convention: the first value corresponds to the central wavelength (in nanometers, nm), which is the midpoint of the light allowed to pass through the filter; the second corresponds to the bandwidth, i.e., the width of this "window" of light. Thus, a 450/45 filter transmits light between 427.5 nm and 472.5 nm (i.e., 450 ± 22.5 nm). In addition to fluorescence, two scatter parameters were recorded to describe particle morphology: grain size and granularity. ~~The forward scatter (FSC) measures light diffracted by the pollen grain at a flat angle, reflecting the approximate diameter of the grain. The sidewards scatter (SSC) measures light diffracted by the pollen grain at a right angle, reflecting its granularity.~~ The forward scatter (FSC) detects light scattered at low angles in the forward direction, which correlates with the cross-sectional area of the particle, equivalent to a spherical diameter. For non-spherical particles like pollen (prolate, oblate, tricolporate, etc.),

FSC reflects an average optical cross-section as the particle passes through the laser in a random orientation. The sidewards scatter (SSC) detects light scattered at ~90° (orthogonal) to the laser beam, which is sensitive to internal complexity and surface irregularities. In pollen, this captures internal granularity, wall sculpturing, apertures, vacuoles/ pollen sacs. The more complex the structure and texture of the pollen grain-, the higher the granularity values will be.

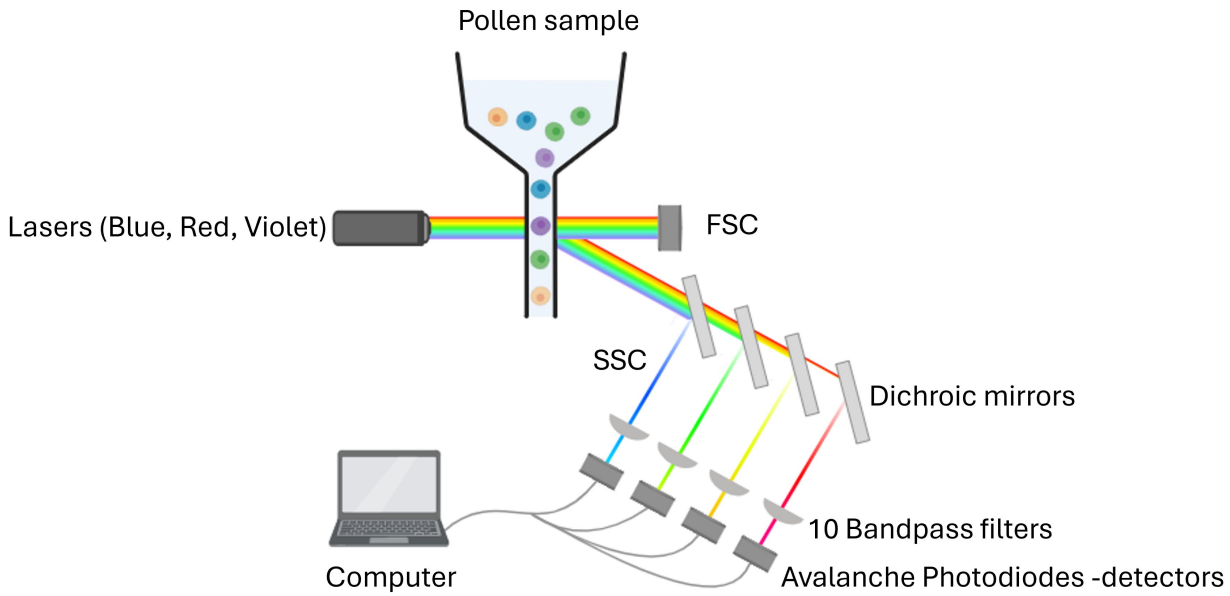

Figure 1: Flow cytometry workflow on the CytoFLEX (Beckman Coulter, Inc.). Sample containing pollen enters at the top, and then is excited by three lasers in the blue (λ=488nm), red (λ=640nm) and violet (λ=405nm) wavelengths, 10 dichroic mirrors, bandpass filters and detectors in different wavelength ranges (λ=450/45, 525/40, 610/20, 585/42, 525/40, 690/50, 780/60, 660/10, 712/25 and 780/60 nm). There are two additional detectors for size and granularity: f~~F~~orward scatter (FSC) and side scatter (SSC). Created with BioRender.

2.3 Data cleaning

Although the samples were filtered to retain only particles within the size range of pollen grains (5-100µm), some non-pollen particles, such as dust or plant debris, were still present. To distinguish pollen from debris, that is non-pollen particles, we used the recorded size, granularity, and fluorescence parameters for each particle. These ~~which~~ include one value for size (FSC), one for granularity (SSC), and ten values for fluorescence, each with two components, the maximum peak height and the peak area except size which has also a width component. ~~This resulted in a total of 25 parameter values per particle.~~ This resulted in

three values for size, two for granularity, and 20 for fluorescence, with a total of 25 parameter values per particle.

Data cleaning was performed using Cytexpert software version 2.4.28 (Beckman Coulter, Inc.). For each species, pollen grains were manually separated from debris using scatter density plots (size vs. granularity) and histograms of all fluorescence features. This selection relied primarily on the PB450 (λ=450/45nm) and Violet610 (λ=610/20nm) fluorescence histograms, while cross-checking against the other recorded parameters to ensure consistency. Adjustments were made as needed to ensure that only true pollen grains were retained (Fig. A2). This excitation/emission range is characteristic of sporopollenin which contains the fluorophores specific to pollen grains (Pöhlker et al., 2013). The final training dataset included all cleaned pollen data from each species along with a separate category, "OTHER", which combined all debris data from the cleaning step and the particles from certain species for which it was impossible to distinguish pollen from debris, such as those in the *Thuja* genus. The final reference database used to train the model comprised 97 species from 34 different genera. A detailed list of species is presented in Table A1 and the complete training datasets are available on Figshare (Tardif, 2025) ~~(https://doi.org/10.6084/m9.figshare.30870641)~~.

2.4 Machine learning algorithm

Four supervised classification algorithms were initially tested: *Random Forest* (Breiman, 2021), *Gradient Boosting*, *Extreme Gradient Boosting* and *Neuronal Network.* Among these, the Random Forest algorithm showed the best performance using F1-scores and was therefore selected for subsequent analysis. In our training dataset, the number of pollen grains varies across taxa (~~min=306; max=35307)~~Table A2). This caused the model to more frequently predict taxa with more training examples (Chawla, 2010). To address this class imbalance, we used the synthetic minority over-sampling technique (Chawla, 2010), resulting in a balanced dataset with 1,000 pollen grains per species for the species-level classification model and 10,000 pollen grains per genus for the genus-level classification model. Only four taxa were oversampled (*Acer saccharum*, *Gramineae spp*, *Juglans cinerea*, and *Picea abies*). The purpose of balancing data was to provide the classifier with a balanced training set to prevent it from being biased toward the majority class. Each dataset was randomly split into two subsets: 70% for training and 30% for validation. The validation set, was not used for model training. The Random Forest classifier was trained exclusively on the 70% training portion. Models were trained using the *train()* function from the *caret* package in R software (version 4.4.0), calling the *rf()* function for the random forest model. Model robustness was assessed using 10-fold cross-validation implemented via the *trainControl()* function with the "cv" method (nine repetitions for training and one for validation). We trained the models using the default value of 500 trees. The

parameter *mtry*, representing the number of variables randomly selected at each node split, was set to 5, based on prior testing across values from 1 to 10. We assessed the models' performance using the F_1-score: F_1= (2*precision*recall)/(precision+recall). Precision is the proportion of correctly predicted positives out of all predicted positives and recall is the proportion of correctly predicted positives out of all actual positives (Grandini et al., 2020). Variable importance was assessed using the mean decrease in Gini coefficient, which quantifies each variable's contribution to reducing classification error by decreasing node impurity during tree construction. The trained models are available on Figshare (Tardif, 2025).

3 Results

3.1 Classification performance

At the species level, the model achieved a mean F_1-score of 0.76 (n=97 species; Fig. 2a). Most species perform very well, with 75% of species achieving a F1-score above 0.70. The lowest F_1-scores were obtained for *Quercus rubra* (0.44), *Salix x pendulina f. tristis.* (*Salix alba tristis* hereafter) (0.43) and *Ulmus minor* (0.44). Several other species also showed reduced accuracy, with F_1-scores ranging between 0.5 and 0.65. These included *Acer x freemanii*, *Acer ukurunduense*, *Fagus grandifolia*, *Fraxinus nigra*, *Pinus banksiana*, and *Syringa villosa*, as well as several species of the Betulaceae family (*Betula papyrifera*, *Carpinus caroliniana*, and *Corylus colurna*), the Juglandaceae family (*Carya ovata*, *Juglans nigra*, and *Juglans virginiana*), and the Ulmus genus (*Ulmus davidiana*, *Ulmus propinqua*, and *Ulmus pumila*) (Fig. 2a).

When trained at the genus level, model performance improved across the 34 genera, reaching a mean F_1-score of 0.90 (Fig. 2b). The only notable exception was *Juglans*, with an F_1-score of 0.73. All other genera achieved F_1-scores close to or above 0.8. Taxa with relatively lower accuracy at the species level, such as those in the genera *Betula*, *Quercus* and *Ulmus*, showed marked improvement at the genus level. Most misclassifications occurred between species within the same genus, as is evident for species from the genus *Ulmus* (see confusion matrices in Appendix B and in supplement material Table S1 and Table S2).

3.2 Variables contribution

The ranking of predictors using the Gini index shows that the most important variables for distinguishing pollen grains among taxa were granularity (SSC), two fluorescence variables from the violet laser (PB450 and Violet610) and one from the blue laser (FITC). These variables exhibited the highest mean decrease in Gini, indicating a major contribution to the homogeneity of nodes and consequently, to overall classification accuracy in the Random Forest model (Fig. 3).

Analysis of the variables contributing most to pollen differentiation revealed that size (FSC) and granularity (SSC) varied more among genera than among species within a given genus, whereas fluorescence parameters primarily accounted for the variation observed among species within genera (Fig.4 and Appendix C). Figure 4 illustrates the distributions for six genera known to be allergenic (see Appendix C for more details). Pollen grains from the *Pinus* genus were larger than those from other genera and also had a specific granularity pattern. For these two parameters, FSC and SSC, intra-genus variation for all genera was very small or absent. In contrast, fluorescence parameters showed more pronounced differences among species within the same genus. For example, *Alnus* species presented distinct values across all three fluorescence channels (FITC, Violet610, PB450), while *Corylus* species differed mainly in the Violet610 channel. For other genera, only certain species, such as *Betula nigra*, *Quercus macrocarpa*, and *Salix spp.*, showed distinct fluorescence profiles (Fig. 4).

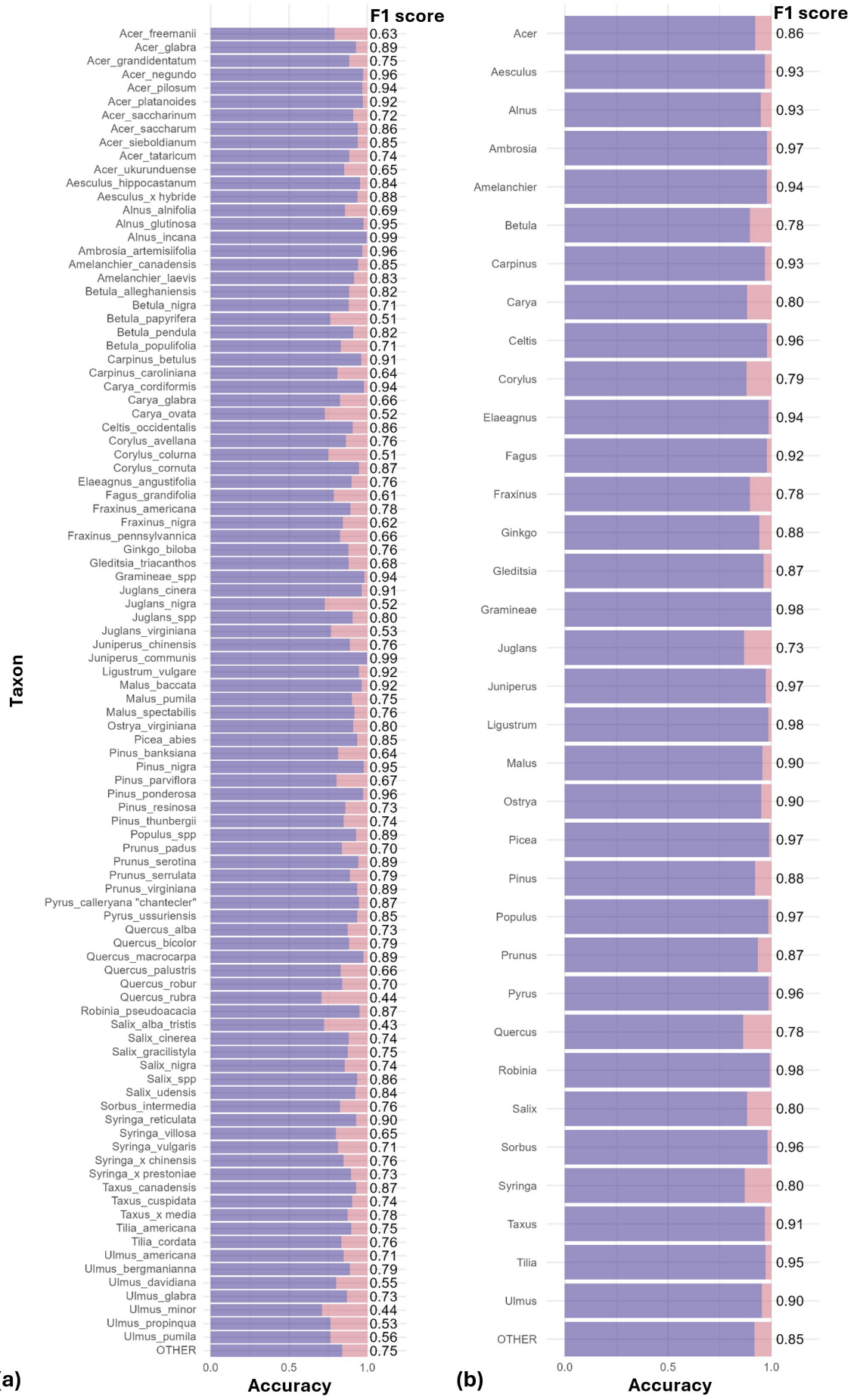
F1 score
Taxon
Acer_freemanii 0.63
Acer_glabra 0.89
Acer_grandidentatum 0.75
Acer_negundo 0.96
Acer_pilosum 0.94
Acer_platanoides 0.92
Acer_saccharinum 0.72
Acer_saccharum 0.86
Acer_sieboldianum 0.85
Acer_tataricum 0.74
Acer_ukurunduense 0.65
Aesculus_hippocastanum 0.84
Aesculus_x hybride 0.88
Alnus_alnifolia 0.69
Alnus_glutinosa 0.95
Alnus_incana 0.99
Ambrosia_artemisiifolia 0.96
Amelanchier_canadensis 0.85
Amelanchier_laevis 0.83
Betula_alleghaniensis 0.82
Betula_nigra 0.71
Betula_papyrifera 0.51
Betula_pendula 0.82
Betula_populifolia 0.71
Carpinus_betulus 0.91
Carpinus_caroliniana 0.64
Carya_cordiformis 0.94
Carya_glabra 0.66
Carya_ovata 0.52
Celtis_occidentalis 0.86
Corylus_avellana 0.76
Corylus_colurna 0.51
Corylus_cornuta 0.87
Elaeagnus_angustifolia 0.76
Fagus_grandifolia 0.61
Fraxinus_americana 0.78
Fraxinus_nigra 0.62
Fraxinus_pennsylvannica 0.66
Ginkgo_biloba 0.76
Gleditsia_triacanthos 0.68
Gramineae_spp 0.94
Juglans_cinera 0.91
Juglans_nigra 0.52
Juglans_spp 0.80
Juglans_virginiana 0.53
Juniperus_chinensis 0.76
Juniperus_communis 0.99
Ligustrum_vulgare 0.92
Malus_baccata 0.92
Malus_pumila 0.75
Malus_spectabilis 0.76
Ostrya_virginiana 0.80
Picea_abies 0.85
Pinus_banksiana 0.64
Pinus_nigra 0.95
Pinus_parviflora 0.67
Pinus_ponderosa 0.96
Pinus_resinosa 0.73
Pinus_thunbergii 0.74
Populus_spp 0.89
Prunus_padus 0.70
Prunus_serotina 0.89
Prunus_serrulata 0.79
Prunus_virginiana 0.89
Pyrus_calleryana "chantecler" 0.87
Pyrus_ussuriensis 0.85
Quercus_alba 0.73
Quercus_bicolor 0.79
Quercus_macrocarpa 0.89
Quercus_palustris 0.66
Quercus_robur 0.70
Quercus_rubra 0.44
Robinia_pseudoacacia 0.87
Salix_alba_tristis 0.43
Salix_cinerea 0.74
Salix_gracilistyla 0.75
Salix_nigra 0.74
Salix_spp 0.86
Salix_udensis 0.84
Sorbus_intermedia 0.76
Syringa_reticulata 0.90
Syringa_villosa 0.65
Syringa_vulgaris 0.71
Syringa_x chinensis 0.76
Syringa_x prestoniae 0.73
Taxus_canadensis 0.87
Taxus_cuspidata 0.74
Taxus_x media 0.78
Tilia_americana 0.75
Tilia_cordata 0.76
Ulmus_americana 0.71
Ulmus_bergmanianna 0.79
Ulmus_davidiana 0.55
Ulmus_glabra 0.73
Ulmus_minor 0.44
Ulmus_propinqua 0.53
Ulmus_pumila 0.56
OTHER 0.75
0.0
0.5
1.0
Accuracy
(a)
F1 score
Acer 0.86
Aesculus 0.93
Alnus 0.93
Ambrosia 0.97
Amelanchier 0.94
Betula 0.78
Carpinus 0.93
Carya 0.80
Celtis 0.96
Corylus 0.79
Elaeagnus 0.94
Fagus 0.92
Fraxinus 0.78
Ginkgo 0.88
Gleditsia 0.87
Gramineae 0.98
Juglans 0.73
Juniperus 0.97
Ligustrum 0.98
Malus 0.90
Ostrya 0.90
Picea 0.97
Pinus 0.88
Populus 0.97
Prunus 0.87
Pyrus 0.96
Quercus 0.78
Robinia 0.98
Salix 0.80
Sorbus 0.96
Syringa 0.80
Taxus 0.91
Tilia 0.95
Ulmus 0.90
OTHER 0.85
0.0
0.5
1.0
Accuracy
(b)

Figure 2: Performance of the classification models at the species (a) and genus levels (b). For each taxon, purple bars represent correct classifications (accuracy) and pink represents misclassifications (1-accuracy). F_1-scores are shown as labels to the right of each bar. Mean F_1-scores were 0.76 for the species-level model and 0.90 for the genus-level model.

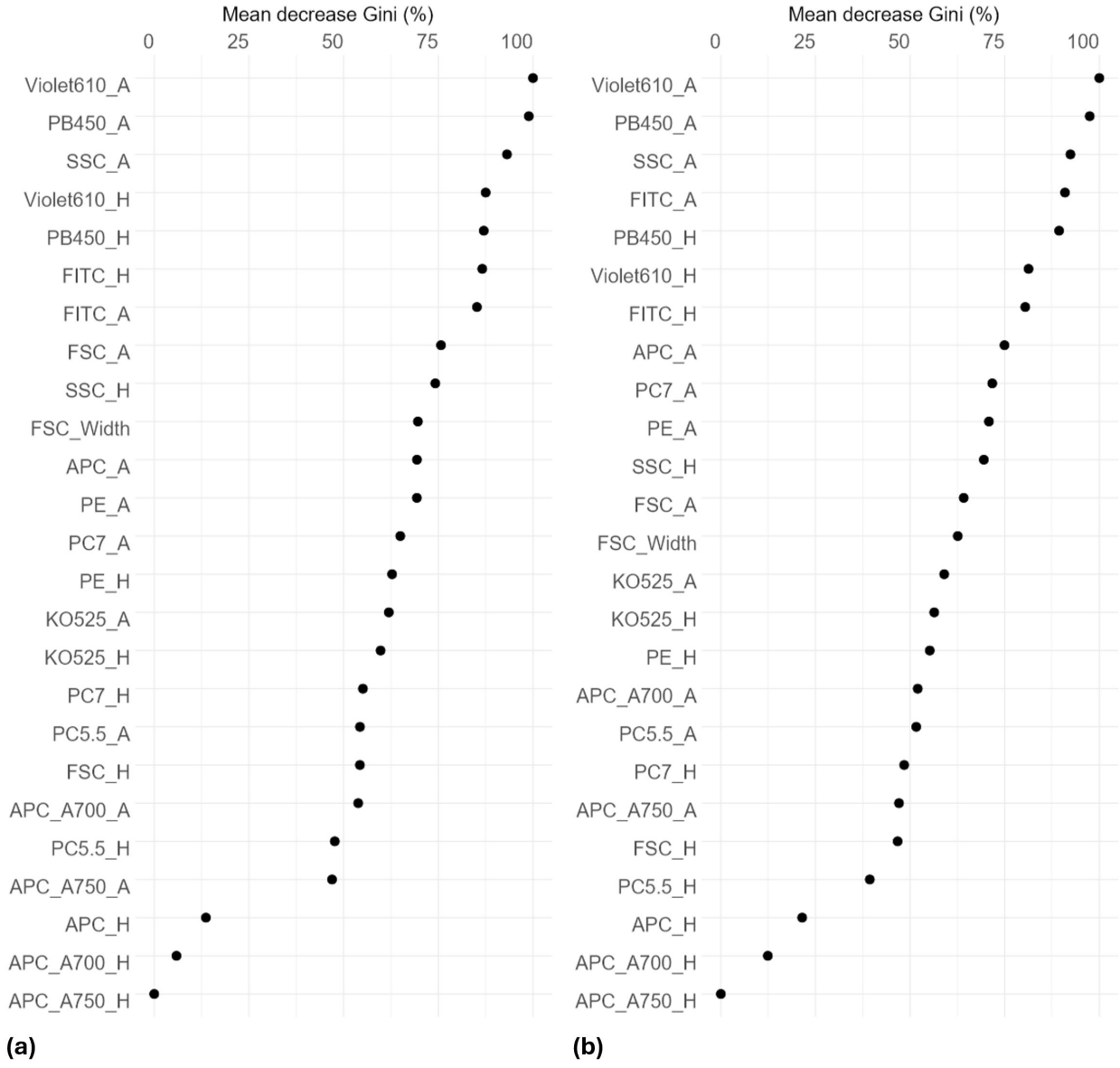

Figure 3: Variable contributions to node and leaf purity in the Rrandom Fforest classification models, measured by mean decrease in Gini index. Higher values indicate greater importance. Results are shown for species-level (a) and genus-level (b) models. Each variable includes two metrics: maximum peak height (H) and peak area (A). Explanation of variable names in FigureA1.

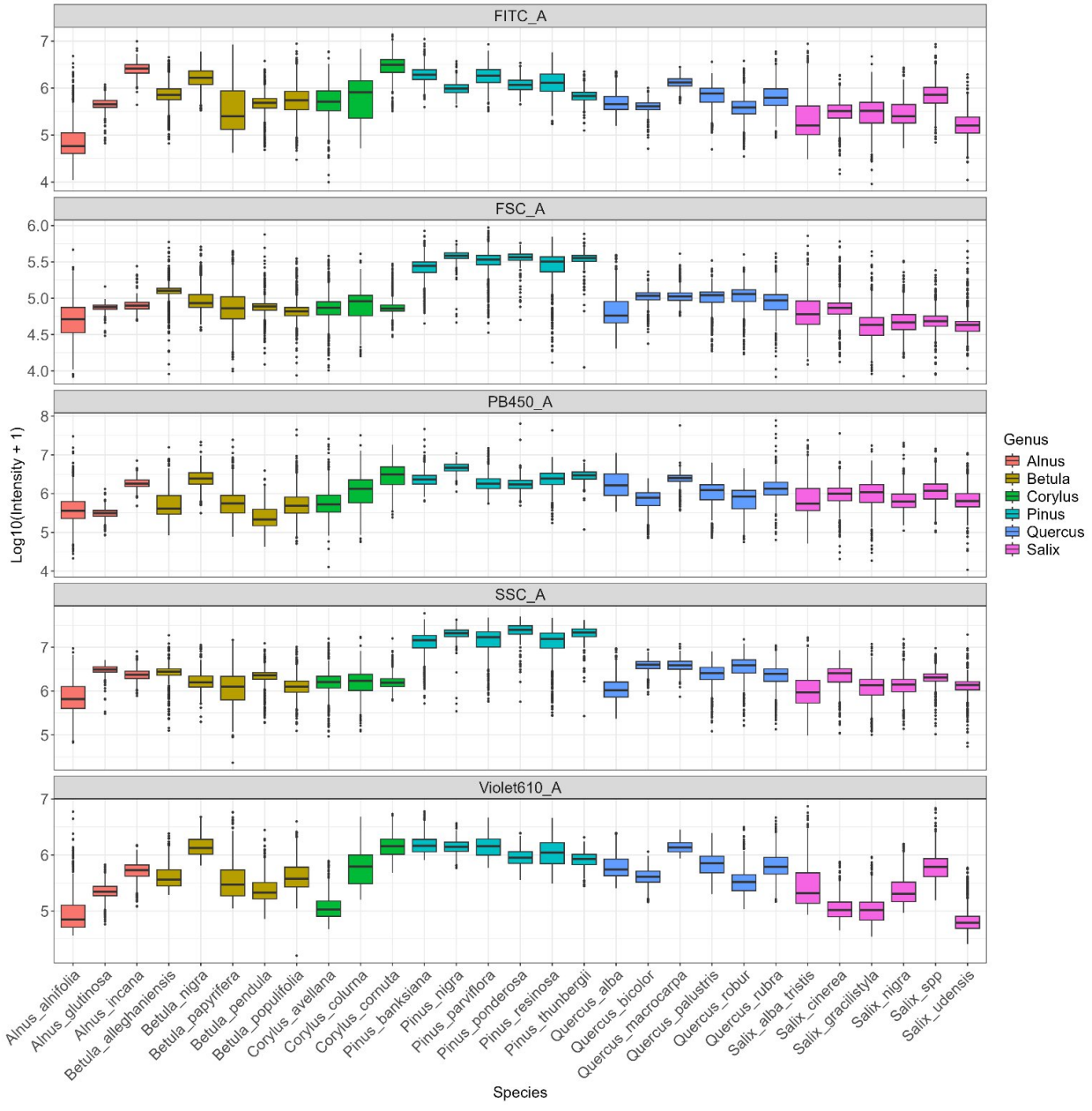

Figure 4: ~~–~~Distribution of log-transformed values for the five variables that contributed the most to distinguish species~~taxa~~. Fluorescence channels: FITC_A (excitation: 488 nm/emission: 525 nm), PB450_A (excitation: 405 nm/ emission: 450 nm), Violet610_A (excitation: 405 nm/ emission: 610 nm); scatter parameters: SSC_A (granularity) and FSC_A (size). The suffix _A indicates that we consider the signal's peak area. Only species from six known allergenic genera (*Alnus*, *Betula*, *Corylus*, *Pinus*, *Quercus*, *Salix*) are shown and coloured. For ~~more~~all species see Appendix C. ~~Colors indicate genus.~~

4 Discussion

Our results demonstrate that flow cytometry combined with machine learning can reliably identify pollen across a wide range of taxa. The models achieved high classification performance (F_1=0.76 at the species level and 0.90 at the genus level) highlighting the potential of this approach as a scalable alternative to traditional microscopy for pollen identification. This represents a significant improvement over conventional methods, such as microscopy, which typically only resolve pollen to the genus or family level. The improved performance of the genus-level model over the species-level model most likely reflects biological and structural similarities among species within the same genus. This was particularly evident for species in the *Betulaceae* family, which are wind-pollinated and considered highly allergenic (D'Amato et al., 2007; Falagiani, 1989), but also for other genera especially abundant in Montreal, such as *Acer*, *Syringa*, and *Ulmus*. While these findings are promising, they were obtained using reference pollen grains collected directly on trees; further validation using atmospheric samples will be necessary before implementation in an airborne pollen monitoring network.

The advantage of flow cytometry coupled with machine learning lies not only in its performance in classifying at the genus or species level, but especially in its ability to enable automated, high-throughput identification (≈5000 grains·s^{-1}) while avoiding the lengthy and costly training required for human specialists. Accurate monitoring is clinically important, as even low pollen concentrations (10–50 grains per cubic meter) can trigger allergic symptoms (Steckling-Muschack et al., 2021). From a public health perspective, the genus-level model is therefore appropriate, as it provides higher accuracy for the taxa most relevant to allergy monitoring.

The fluorescence variables that contributed most to pollen classification were associated with blue and violet excitation lasers, with emission detected in the blue (PB450), red-orange (Violet610), and green (FITC) channels. This pattern is consistent with the known autofluorescence properties of sporopollenin, the main biopolymer in the pollen exine, which emits strongly near 475 nm (Pöhlker et al., 2013). Additional emissions likely originate from secondary compounds such as flavonoids, carotenoids, and terpenes located in the exine or pollenkitt coating (Donaldson, 2020; Pöhlker et al., 2013). The distribution of the most discriminative variables indicates that size and granularity primarily differentiate genera, while blue, red-orange and green fluorescence channels capture species-level differences within genera. This pattern explains the model's higher accuracy at the genus-level and its partial success in distinguishing closely related species. The misclassifications at species-level likely stem from the high similarity in pollen ~~size~~shape and fluorescence spectra among closely related species, which makes them harder to distinguish. In addition, because our classification relied on size and fluorescence alone, without complementary

morphological data such as holography images (Erb et al., 2024; Gierlicka et al., 2022; Zhang and Abdulla, 2023), the model's performance may have been constrained by limited representation of some taxa in the reference dataset. Increasing both the number of pollen grains per species and the diversity of species within each genus would help train more robust models. Future research should prioritize expanding reference datasets, ideally through the creation of a global database of pollen fluorescence signatures, which represent the emission spectrum for given excitation wavelengths. Such a resource, similar to *The Global Pollen Project*, for microscopic images (Martin and Harvey, 2017), would provide a valuable foundation for machine learning and deep leaning applications in aerobiology, but also ecology, palynology, paleoecology, and other pollen related fields.

Another factor that may explain the reduced model accuracy is that some species in our reference collection could not be included in the model's training dataset due to the impossibility to distinguish pollen from debris during the data cleaning, even though we had visually confirmed the presence of intact pollen grains in our samples. These data were included in the training dataset under the category "OTHER" rather than assigned to individual taxa. Such was the case for *Thuja*, a genus abundant in Montreal (Paquette et al., 2026), likely due to the small size of its pollen grains, which can easily mix with debris or because pollen grains included in our dataset may have been limited in quantity or had not fully matured. Indeed, distinguishing male from female *Thuja* cones and assessing the phenological stage to collect mature pollen is difficult, and the small size of the cones is another challenge for pollen extraction. Improving collection and extraction protocols for this genus could help reduce debris contamination in future sampling.

A crucial next step is to adapt these models for use on complex airborne samples collected in urban environments. Such samples often contain large amounts of debris as during atmospheric transport, pollen grains may remain airborne for days or weeks, during which they can fold, crack, or adhere to air pollutants (De Weger et al., 2024). They are also exposed to ultraviolet radiation and humidity fluctuations that can alter fluorescence properties. These factors complicate the discrimination of true pollen grains from other particles and represent a major challenge for operational implementation.

Because small pollen grains, folded grains and debris can have overlapping size distributions, misclassification remains a possibility, with pollen occasionally identified as debris, and vice versa. Future research could therefore explore multidimensional hierarchical classification frameworks, especially when complementarity data such as holographic images are available for validation. For example, when classification confidence is high, the model could assign a species-level label, but default to a broader taxonomic category such as genus or family when uncertainty is greater (Hernández et al., 2014). This

flexibility would prevent incorrect fine-level classifications and improve overall reliability under complex environmental conditions.

Another limitation of flow cytometry-based models concerns their device dependency, as fluorescence intensity values are typically linked to the specific cytometer used during model training, which limits model transferability across instruments and comparison to other measurement. However, deployment within harmonized analyzers is feasible under standard bead-based daily QC protocols (CS&T/Application Settings for conventional analyzers; SpectroFlo QC beads for spectral systems), which have been shown to control inter-instrument MFI drift within single-digit percentages (Cornel et al., 2020; Omana-Zapata et al., 2019; Solly et al., 2013b). Channel-wise normalization during data processing further reduces residual variability, and a lightweight domain-adaptation step, based on acquiring a small reference pollen set on the target instrument, can re-anchor feature distributions prior to inference. FSC and SSC parameters remain more sensitive to flow-rate and optical alignment and should therefore be monitored carefully. Where direct comparison between instruments is required, ERF/MESF calibration from NIST's Flow Cytometry Standards Consortium allows comparing fluorescence results between different instruments (Wang and Hoffman, 2017). Standardization procedures, such as calibrating cytometers using Rainbow beads and Quality Control beads could help ensure consistent signal outputs across different instruments (Solly et al., 2013). The present work was carried out using a conventional cytometer with three lasers and ten filters; using equipment with more lasers and detectors could refine the detection of fluorescent signatures and detect more of them. Spectral cytometry also opens up new possibilities for analyzing fluorescent signatures on a larger scale (Konecny et al., 2024), which could enable even better characterization of pollen based on its fluorescence.

The combination of flow cytometry and a Random Forest classification model proves to be a highly promising approach for the identification of airborne pollen in urban environments. By relying exclusively on routinely measured cytometric parameters, rather than images, this method ensures broad applicability and compatibility with standard healthcare and clinical cytometers. Integrating this approach into existing aerobiological monitoring networks could enable fasternear-real-time identification and quantification of allergenic pollen. We also built an extensive reference pollen collection comprising 97 species across 34 genera. For each species, we have several floral units (flower, catkins, cones) containing pollen, microscopic slides, and flow cytometry data for all pollen grains. This reference collection could be reused for different purposes such as future model training.

5 Conclusion

This study demonstrates a significant advancement in pollen identification by combining flow cytometry with a Rrandom Fforest classification model. This approach achieved high accuracy at both the genus (F_1 = 0.90) and species levels (F_1 = 0.76), surpassing several limitations of traditional microscopy. While species-level classification remains challenging for certain taxa, the results highlight the method's robustness and potential for large-scale implementation. With continued refinement and standardization, this approach could enable fasternear-real-time, cheap, high throughput pollen identification and broaden its applications in aerobiological monitoring, while supporting public health applications and advancing research in pollen ecology worldwide.

6 Code availability

The code is available on the public Github repository SarahTardif/Pollen-classification-model.

7 Data availability

Training datasets and trained models are available on a Figshare repository (https://doi.org/10.6084/m9.figshare.30870641). More data can be provided upon request.

8 Author contribution

ST: conceptualization, data collection, analyses, writing – original draft; AP, ILL, and RSS: conceptualization, funding acquisition, supervision, validation, support, writing – review and editing; GB: mMethodology (cytometry), writing – review and editing; MRK: mMethodology (lab protocols), writing – review and editing; GL: mMethodology (initial algorithm for the machine learning model), writing – review and editing

9 Competing interests

The authors declare that they have no conflict of interest.

10 Acknowledgements

We thank the CERMO-UQAM Imaging Platform and the Aerobiology Research Laboratories for their technical support. We are grateful for the precious help of Kira Safranova, Emily Ducharme, Maya Héon, and Kim Florentin in sampling, filtering, and running fresh pollen through the cytometer. We thank the Montreal Botanical Garden for permitting pollen collection from tree flowers. Model training was performed on supercomputers managed by Calcul Québec and the Digital Research Alliance of Canada.

11 Financial support

This work was funded by NSERC-Alliance ALLRP 554373 – 21 and *Fonds vert dans le cadre du Plan d'action 2013-2020 sur les changements climatiques du gouvernement québécois* awarded to AP.

ST also received funding from the Urban forestry program NSERC-CREATE -543300-20.

Appendix A: Reference pollen collection

Table A1: Species in the reference pollen collection

Family	Genus	Species (scientific name)	Authority
Asteraceae	*Ambrosia*	*Ambrosia artemisiifolia*	L.
Betulaceae	*Alnus*	*Alnus alnifolia*	Mill.
		Alnus glutinosa	(L.) Gaertn.
		Alnus incana	(L.) Moench
	Betula	*Betula alleghaniensis*	Britton
		Betula nigra	L.
		Betula papyrifera	Marshall
		Betula pendula	Roth
		Betula populifolia	Marshall
	Carpinus	*Carpinus betulus*	L.
		Carpinus caroliniana	Walter
	Corylus	*Corylus avellana*	L.
		Corylus colurna	L.
		Corylus cornuta	Marshall
	Ostrya	*Ostrya virginiana*	(Mill.) K.Koch
Cannabacées	*Celtis*	*Celtis occidentalis*	L.
Cupressaceae	*Juniperus*	*Juniperus chinensis*	L.
		Juniperus communis	L.
Elaeagnaceae	*Elaeagnus*	*Elaeagnus angustifolia*	L.
Fabaceae	*Gleditsia*	*Gleditsia triacanthos*	L.
	Robinia	*Robinia pseudoacacia*	L.
Fagaceae	*Fagus*	*Fagus grandifolia*	Ehrh.
	Quercus	*Quercus alba*	L.
		Quercus bicolor	Willd.
		Quercus macrocarpa	Michx.
		Quercus palustris	Mnchh.
		Quercus robur	L.
		Quercus rubra	L.
Ginkgoaceae	*Ginkgo*	*Ginkgo biloba*	L.
Gramineae/Poaceae	-	*Gramineae spp*	
Juglandaceae	*Carya*	*Carya cordiformis*	(Wangenh.) K.Koch
		Carya glabra	(Mill.) Sweet
		Carya ovata	(Mill.) K.Koch
	Juglans	*Juglans cinerea*	L.
		Juglans nigra	L.
		Juglans spp	L.
		Juglans virginiana	L.

363

Family	Genus	Species (scientific name)	Authority¤
Oleaceae	*Fraxinus*	*Fraxinus americana*	L.
		Fraxinus nigra	Marshall
		Fraxinus pennsylvannica	Marshall
	Ligustrum	*Ligustrum vulgare*	L.
	Syringa	*Syringa reticulata*	(Blume) H.Hara
		Syringa villosa	Vahl
		Syringa vulgaris	L.
		Syringa x chinensis	Willd.
		Syringa x prestoniae	McKelvey
Pinaceae	*Picea*	*Picea abies*	(L.) H.Karst.
	Pinus	*Pinus banksiana*	Lamb.
		Pinus nigra	J.F.Arnold
		Pinus parviflora	Siebold & Zucc.
		Pinus ponderosa	Douglas ex C.Lawson
		Pinus resinosa	Aiton
		Pinus thunbergii	Parl.
Rosaceae	*Amelanchier*	*Amelanchier canadensis*	(L.) Medik.
		Amelanchier laevis	Wiegand
	Malus	*Malus baccata*	(L.) Borkh.
		Malus pumila	Mill.
		Malus spectabilis	(Aiton) Borkh.
	Prunus	*Prunus padus*	L.
		Prunus serotina	Ehrh.
		Prunus serrulata	Lindl.
		Prunus virginiana	L.
	Pyrus	*Pyrus calleryana "chantecler"*	Decne.
		Pyrus ussuriensis	Maxim.
	Sorbus	*Sorbus intermedia*	Ehrh.
Salicaceae	*Populus*	*Populus spp*	L.
	Salix	*Salix alba tristis*	Gaudin
		Salix cinerea	L.
		Salix gracilistyla	Miq.
		Salix nigra	Marshall
		Salix spp	
		Salix udensis	(Wimm.) Trautv. & C.A.Mey.

364

Family	Genus	Species (scientific name)	Authority¤
Sapindaceae	*Acer*	*Acer freemanii*	A.E.Murray
		Acer glabra	Torr.
		Acer grandidentatum	Nutt. ex Torr. & A.Gray
		Acer negundo	L.
		Acer pilosum	Maxim.
		Acer platanoides	L.
		Acer saccharinum	L.
		Acer saccharum	Marshall
		Acer sieboldianum	Miq.
		Acer tataricum	L.
		Acer ukurunduense	Trautv. & C.A.Mey.
	Aesculus	*Aesculus hippocastanum*	L.
		Aesculus x hybride	DC.
Taxaceae	*Taxus*	*Taxus canadensis*	Marshall
		Taxus cuspidata	Siebold & Zucc.
		Taxus x media	Rehder
Tiliaceae	*Tilia*	*Tilia americana*	L.
		Tilia cordata	Mill.
Ulmaceae	*Ulmus*	*Ulmus americana*	L.
		Ulmus bergmanianna	C.K.Schneid.
		Ulmus davidiana	Planch.
		Ulmus glabra	Huds.
		Ulmus minor	Mill.
		Ulmus propinqua	Koidz.
		Ulmus pumila	L.

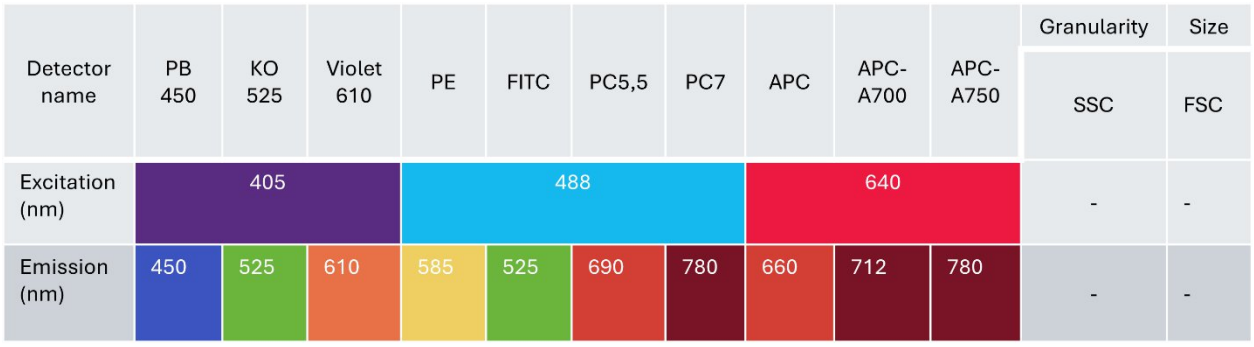

Figure A1: Explanation of cytometry variable names, showing the respective excitation lasers and emission detectors with their wavelengths and associated colors.

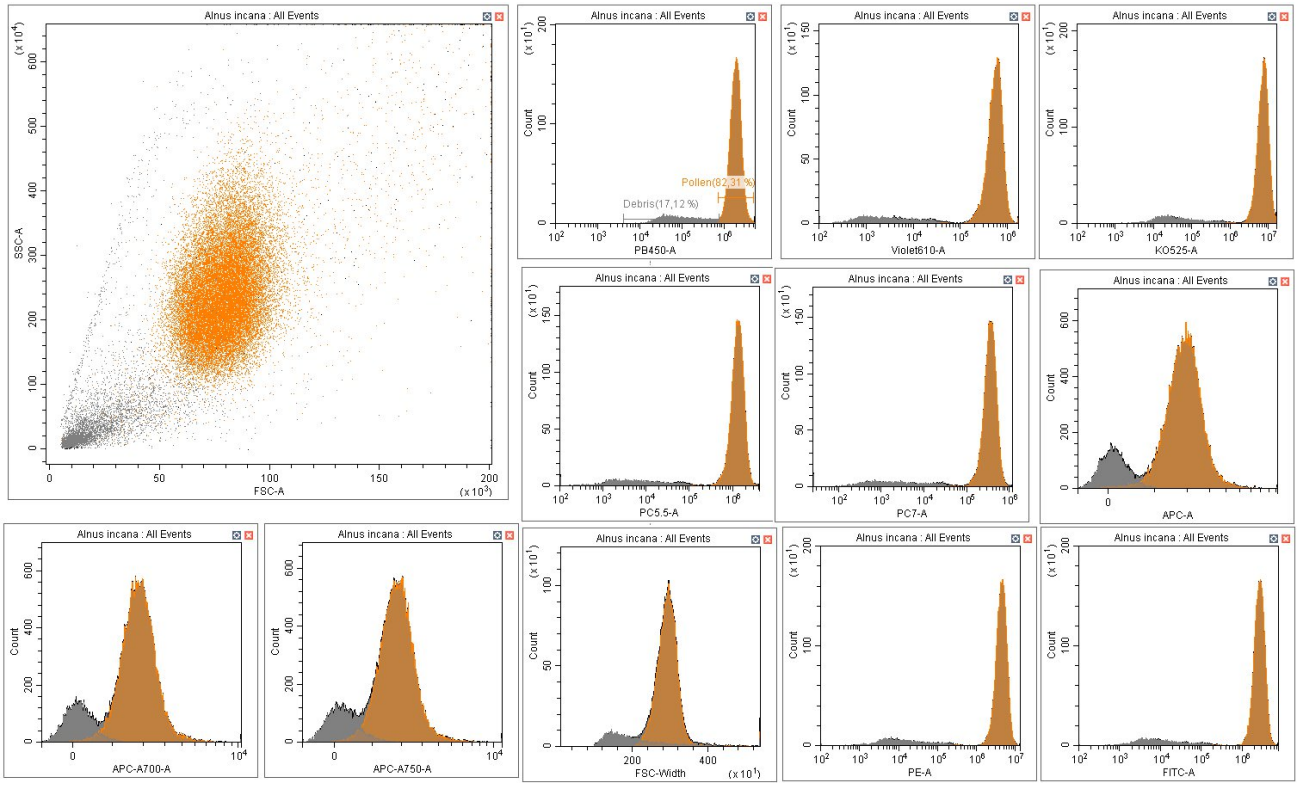

Figure A2: Distinction pollen (orange) versus debris (grey) on CytExpert software: Example of *Alnus incana*

Table A2: Number of pollen grains per species in the training dataset before balancing data¶

Species¤	Freq_pollen
Acer_freemanii¤	2095
Acer_glabra¤	8259
Acer_grandidentatum¤	4324
Acer_negundo¤	15603
Acer_pilosum¤	9220
Acer_platanoides¤	2726
Acer_saccharinum¤	3674
Acer_saccharum¤	447
Acer_sieboldianum¤	11089
Acer_tataricum¤	2605
Acer_ukurunduense¤	3860
Aesculus_hippocastanum¤	8278
Aesculus_x hybride¤	11041
Alnus_alnifolia¤	10517
Alnus_glutinosa¤	21586
Alnus_incana¤	28158

Ambrosia_artemisiifolia¤	33615
Amelanchier_canadensis¤	1552
Amelanchier_laevis¤	3836
Betula_alleghaniensis¤	5780
Betula_nigra¤	4954
Betula_papyrifera¤	13163
Betula_pendula¤	2151
Betula_populifolia¤	21222
Carpinus_betulus¤	2973
Carpinus_caroliniana¤	1580
Carya_cordiformis¤	9603
Carya_glabra¤	3256
Carya_ovata¤	7579
Celtis_occidentalis¤	3238
Corylus_avellana¤	10290
Corylus_colurna¤	4404
Corylus_cornuta¤	1232
Elaeagnus_angustifolia¤	2998
Fagus_grandifolia¤	1428
Fraxinus_americana¤	3689
Fraxinus_nigra¤	2759
Fraxinus_pennsylvannica¤	8732
Ginkgo_biloba¤	12685
Gleditsia_triacanthos¤	7674
Gramineae_spp¤	988
Juglans_cinerea¤	306
Juglans_nigra¤	9867
Juglans_spp¤	11972
Juglans_virginiana¤	2886
Juniperus_chinensis¤	5544
Juniperus_communis¤	35307
Ligustrum_vulgare¤	4278
Malus_baccata¤	2328
Malus_pumila¤	3141
Malus_spectabilis¤	6241
Ostrya_virginiana¤	26203
Picea_abies¤	881
Pinus_banksiana¤	2722
Pinus_nigra¤	14008
Pinus_parviflora¤	2897
Pinus_ponderosa¤	1991
Pinus_resinosa¤	7670
Pinus_thunbergii¤	2751
Populus_spp¤	4720

Prunus_padus¤	1407
Prunus_serotina¤	1878
Prunus_serrulata¤	5575
Prunus_virginiana¤	1242
Pyrus_calleryana "chantecler"¤	1685
Pyrus_ussuriensis¤	1042
Quercus_alba¤	11635
Quercus_bicolor¤	17603
Quercus_macrocarpa¤	13868
Quercus_palustris¤	8956
Quercus_robur¤	23812
Quercus_rubra¤	6899
Robinia_pseudoacacia¤	1828
Salix_alba_tristis¤	7484
Salix_cinerea¤	7372
Salix_gracilistyla¤	6600
Salix_nigra¤	11276
Salix_spp¤	7741
Salix_udensis¤	18766
Sorbus_intermedia¤	1472
Syringa_reticulata¤	2351
Syringa_villosa¤	10681
Syringa_vulgaris¤	8695
Syringa_x chinensis¤	11478
Syringa_x prestoniae¤	11520
Taxus_canadensis¤	4181
Taxus_cuspidata¤	19143
Taxus_x media¤	17655
Tilia_americana¤	3428
Tilia_cordata¤	8802
Ulmus_americana¤	3622
Ulmus_bergmanianna¤	1337
Ulmus_davidiana¤	1050
Ulmus_glabra¤	1340
Ulmus_minor¤	1905
Ulmus_propinqua¤	5762
Ulmus_pumila¤	8377
OTHER¤	100000

372

Appendix B: Confusion matrices

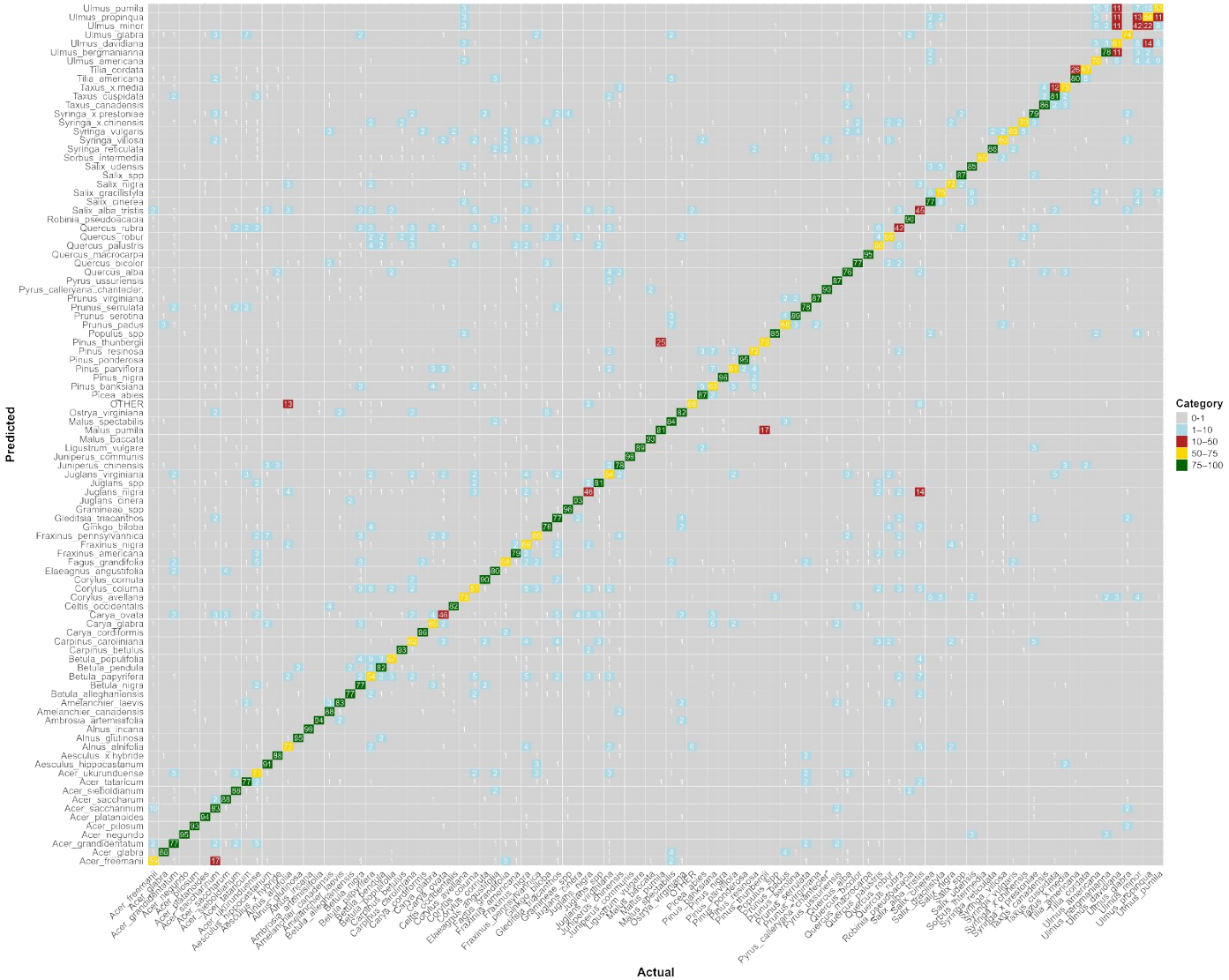

Figure B1: Confusion matrix for the species-level model. The values represent, for each species, the percentage of pollen grains correctly classified (on the diagonal) and misclassified with the actual corresponding species (on the x-axis). Colors correspond to categories (0–1% in gray, 1–10% in blue, 10–50% in red, 50–75% in yellow, and 75–100% in green). Raw data are provided in supplement material Table S1.

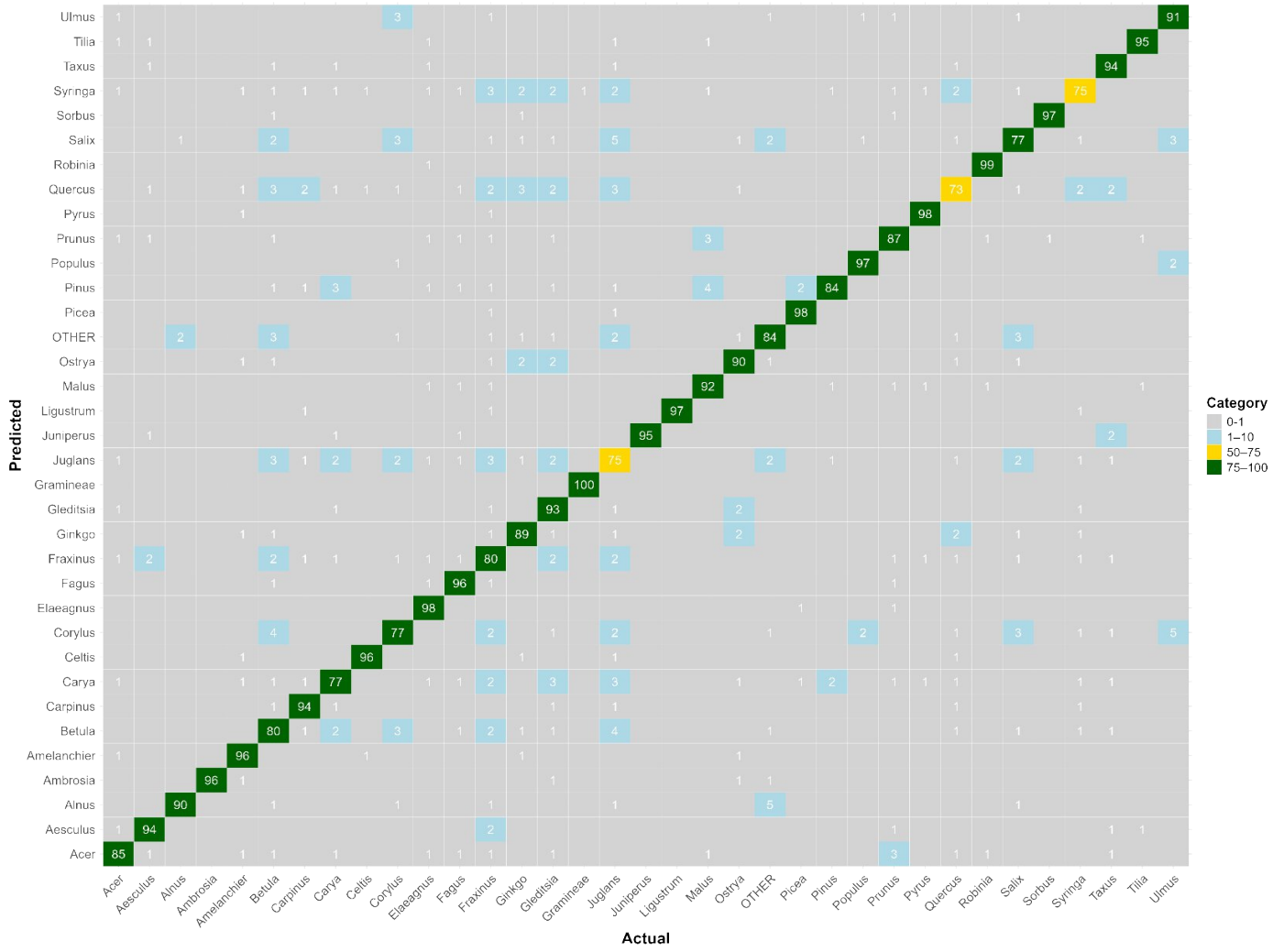

Figure B2: Confusion matrix for the genus-level model. The values represent, for each genus, the percentage of pollen grains correctly classified (on the diagonal) and misclassified with the actual corresponding genus (on the x-axis). Colors correspond to categories (0–1% in gray, 1–10% in blue, 10–50% in red, 50–75% in yellow, and 75–100% in green). Raw data are provided in supplement material Table S2.

Appendix C: Distributions of values for the main discriminant variables.

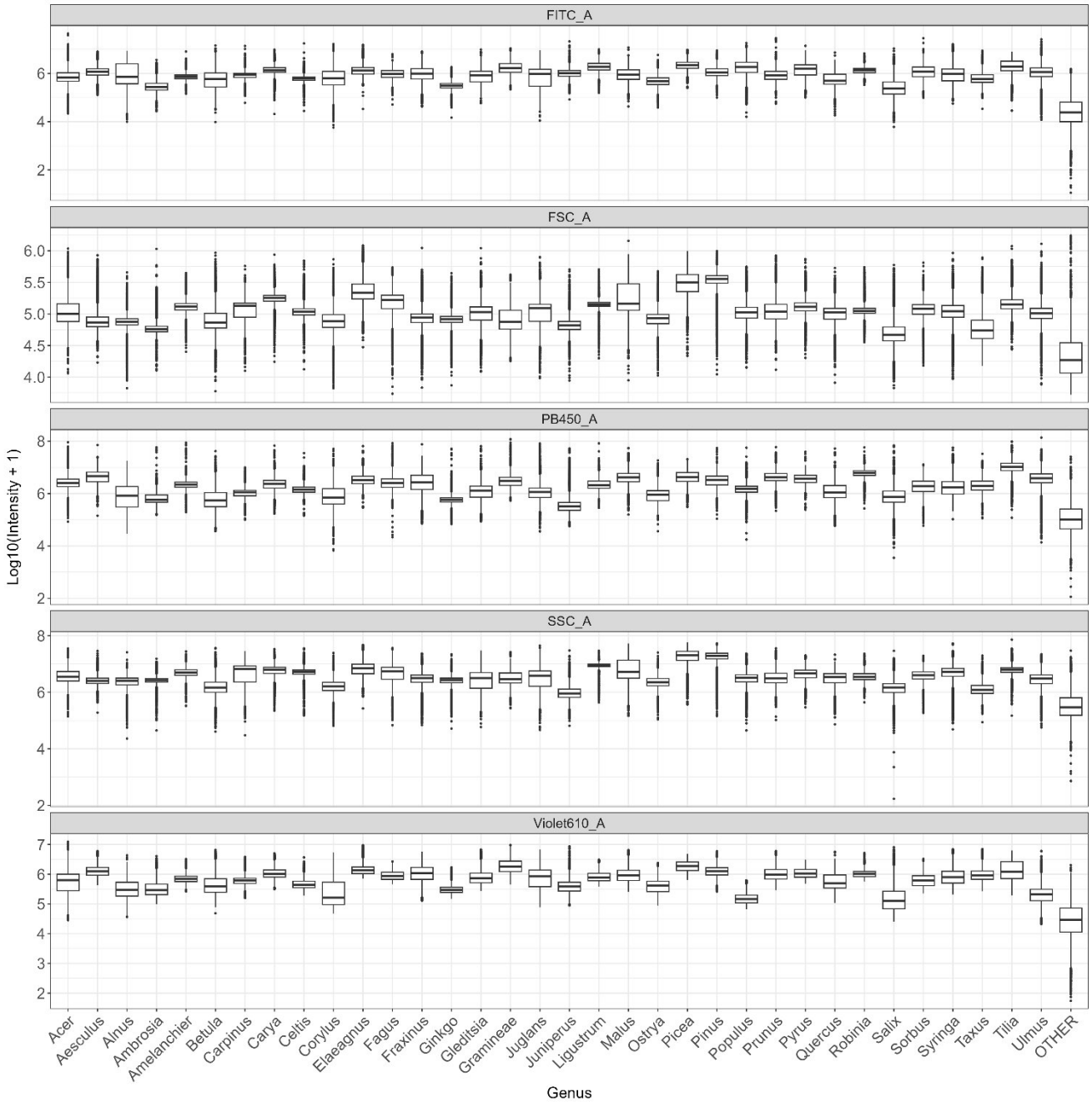

Figure C1: Distribution of log-transformed values for the variables that contribute the most to distinguish taxa (FITC,FSC,SSC,Violet610, PB450) across all genera.

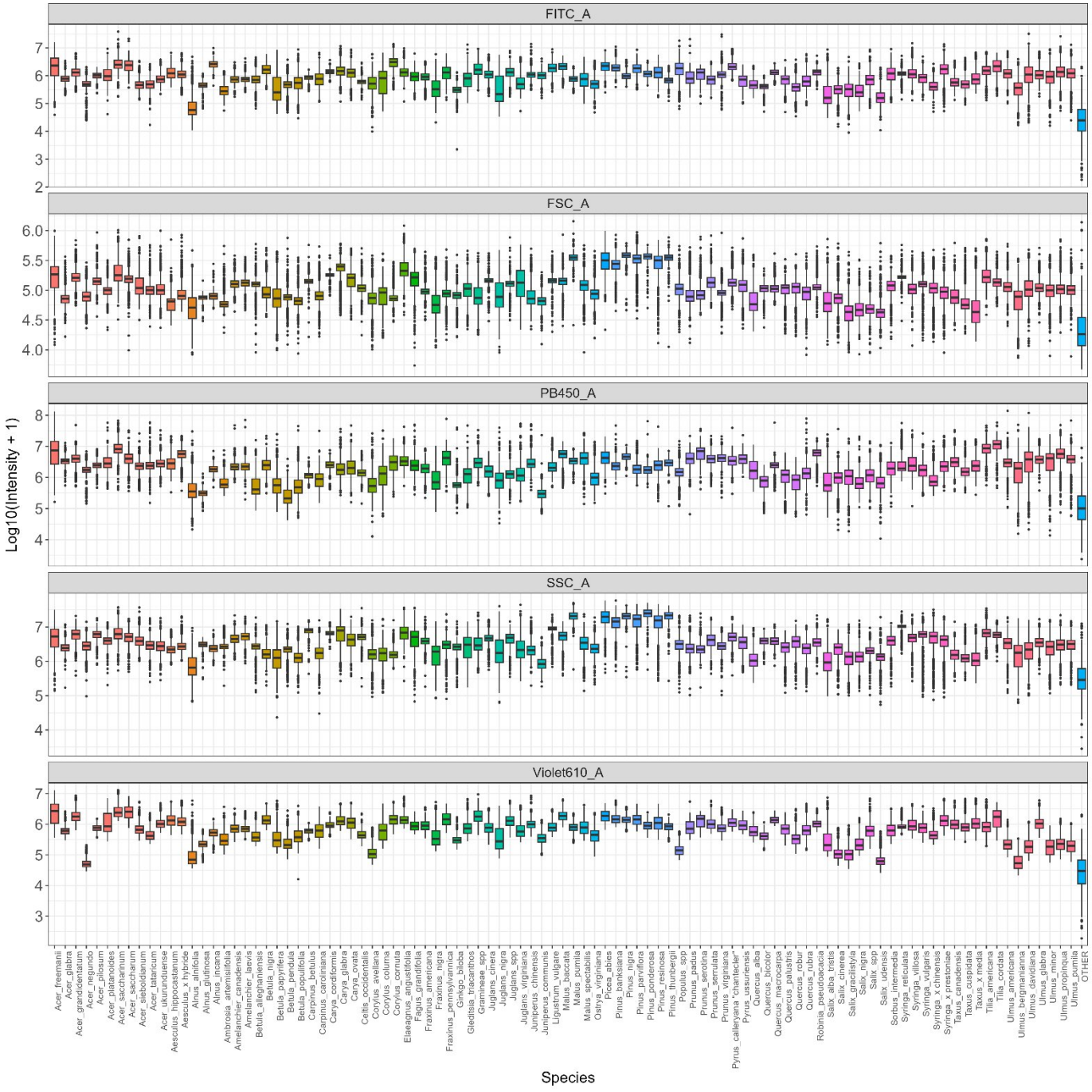

Figure C2: Distribution of log-transformed values for the variables that contribute the most to distinguish taxa (FITC,FSC,SSC,Violet610, PB450) across all species. Colors indicate genus.

References

Ahlholm, Helander, and Savolainen: Genetic and environmental factors affecting the allergenicity of birch (Betula pubescens ssp. czerepanovii [Orl.] Hämet-Ahti) pollen, Clinical & Experimental Allergy, 28, 1384–1388, https://doi.org/10.1046/j.1365-2222.1998.00404.x, 1998.

Aloisi, I., Cai, G., Tumiatti, V., Minarini, A., and Del Duca, S.: Natural polyamines and synthetic analogs modify the growth and the morphology of Pyrus communis pollen tubes affecting ROS levels and causing cell death, Plant Science, 239, 92–105, https://doi.org/10.1016/j.plantsci.2015.07.008, 2015.

Anderegg, W. R. L., Abatzoglou, J. T., Anderegg, L. D. L., Bielory, L., Kinney, P. L., and Ziska, L.: Anthropogenic climate change is worsening North American pollen seasons, Proc. Natl. Acad. Sci. U.S.A., 118, e2013284118, https://doi.org/10.1073/pnas.2013284118, 2021.

Breiman, L.: Random forests. Machine learning, 2001.

Brennan, G. L., Potter, C., de Vere, N., Griffith, G. W., Skjøth, C. A., Osborne, N. J., Wheeler, B. W., McInnes, R. N., Clewlow, Y., Barber, A., Hanlon, H. M., Hegarty, M., Jones, L., Kurganskiy, A., Rowney, F. M., Armitage, C., Adams-Groom, B., Ford, C. R., Petch, G. M., and Creer, S.: Temperate airborne grass pollen defined by spatio-temporal shifts in community composition, Nat Ecol Evol, 3, 750–754, https://doi.org/10.1038/s41559-019-0849-7, 2019.

Chawla, N. V.: Data mining for imbalanced datasets: An overview, in: Data mining and knowledge discovery handbook, 875–886, 2010.

Cornel, A. M., Van Der Burght, C. A. J., Nierkens, S., and Van Velzen, J. F.: FACSCanto II and LSRFortessa flow cytometer instruments can be synchronized utilizing single-fluorochrome–conjugated surface-dyed beads for standardized immunophenotyping, Clinical Laboratory Analysis, 34, e23361, https://doi.org/10.1002/jcla.23361, 2020.

D'Amato, G., Cecchi, L., Bonini, S., Nunes, C., Annesi-Maesano, I., Behrendt, H., Liccardi, G., Popov, T., and van Cauwenberge, P.: Allergenic pollen and pollen allergy in Europe, Allergy, 62, 976–990, https://doi.org/10.1111/j.1398-9995.2007.01393.x, 2007.

De Weger, L. A., Bergmann, K. Ch., Rantio-Lehtimäki, A., Dahl, A., Buters, J., Déchamp, C., Belmonte, J., Thibaudon, M., Cecchi, L., Besancenot, J.-P., Galán, C., and Waisel, Y.: Impact of Pollen, in: Allergenic Pollen: A Review of the Production, Release, Distribution and Health Impacts, 161,203, 2013.

De Weger, L. A., Verbeek, C., Markey, E., O'Connor, D. J., and Gosling, W. D.: Greater difference between airborne and flower pollen chemistry, than between pollen collected across a pollution gradient in the Netherlands, Science of The Total Environment, 934, 172963, https://doi.org/10.1016/j.scitotenv.2024.172963, 2024.

Donaldson, L.: Autofluorescence in Plants, Molecules, 25, 2393, https://doi.org/10.3390/molecules25102393, 2020.

Dunker, S., Boyd, M., Durka, W., Erler, S., Harpole, W. S., Henning, S., Herzschuh, U., Hornick, T., Knight, T., Lips, S., Mäder, P., Švara, E. M., Mozarowski, S., Rakosy, D., Römermann, C., Schmitt-Jansen, M., Stoof-Leichsenring, K., Stratmann, F., Treudler, R., Virtanen, R., Wendt-Potthoff, K., and Wilhelm, C.: The potential of multispectral imaging flow cytometry for environmental monitoring, Cytometry Pt A, 101, 782–799, https://doi.org/10.1002/cyto.a.24658, 2022.

Dunker, S., Motivans, E., Rakosy, D., Boho, D., Mäder, P., Hornick, T., and Knight, T. M.: Pollen analysis using multispectral imaging flow cytometry and deep learning, New Phytologist, 229, 593–606, https://doi.org/10.1111/nph.16882, 2021.

Erb, S., Graf, E., Zeder, Y., Lionetti, S., Berne, A., Clot, B., Lieberherr, G., Tummon, F., Wullschleger, P., and Crouzy, B.: Real-time pollen identification using holographic imaging and fluorescence measurements, Atmos. Meas. Tech., 17, 441–451, https://doi.org/10.5194/amt-17-441-2024, 2024.

Falagiani, P.: Pollinosis, CRC Press, 288 pp., 1989.

Gierlicka, I., Kasprzyk, I., and Wnuk, M.: Imaging Flow Cytometry as a Quick and Effective Identification Technique of Pollen Grains from Betulaceae, Oleaceae, Urticaceae and Asteraceae, Cells, 11, 598, https://doi.org/10.3390/cells11040598, 2022.

Grandini, M., Bagli, E., and Visani, G.: Metrics for Multi-Class Classification: an Overview, https://doi.org/10.48550/arXiv.2008.05756, 13 August 2020.

Hernández, J., Sucar, L. E., and Morales, E. F.: Multidimensional hierarchical classification, Expert Systems with Applications, 41, 7671–7677, https://doi.org/10.1016/j.eswa.2014.05.054, 2014.

Holt, K. A. and Bennett, K. D.: Principles and methods for automated palynology, New Phytologist, 203, 735–742, https://doi.org/10.1111/nph.12848, 2014.

Kim, K. R., Oh, J.-W., Woo, S.-Y., Seo, Y. A., Choi, Y.-J., Kim, H. S., Lee, W. Y., and Kim, B.-J.: Does the increase in ambient CO2 concentration elevate allergy risks posed by oak pollen?, Int J Biometeorol, 62, 1587–1594, https://doi.org/10.1007/s00484-018-1558-7, 2018.

Konecny, A. J., Mage, P. L., Tyznik, A. J., Prlic, M., and Mair, F.: OMIP-102: 50-color phenotyping of the human immune system with in-depth assessment of T cells and dendritic cells, Cytometry Part A, 105, 430–436, https://doi.org/10.1002/cyto.a.24841, 2024.

Ladeau, S. L. and Clark, J. S.: Pollen production by Pinus taeda growing in elevated atmospheric CO 2, Functional Ecology, 20, 541–547, https://doi.org/10.1111/j.1365-2435.2006.01133.x, 2006.

Martin, A. C. and Harvey, W. J.: The Global Pollen Project: a new tool for pollen identification and the dissemination of physical reference collections, Methods Ecol Evol, 8, 892–897, https://doi.org/10.1111/2041-210X.12752, 2017.

Medek, D. E., Katelaris, C. H., Milic, A., Beggs, P. J., Lampugnani, E. R., Vicendese, D., Erbas, B., and Davies, J. M.: Aerobiology matters: Why people in the community access pollen information and how they use it, Clinical & Translational All, 15, e70031, https://doi.org/10.1002/clt2.70031, 2025.

Mousavi, F., Oteros, J., Shahali, Y., and Carinanos, P.: Impacts of climate change on allergenic pollen production: A systematic review and meta-analysis, Agricultural and Forest Meteorology, 349, 109948, https://doi.org/10.1016/j.agrformet.2024.109948, 2024.

Ogden, E. C., Museum, N. Y. S., Service, S., and Commission, U. S. A. E.: Manual for Sampling Airborne Pollen, Hafner Press, 1974.

Omana-Zapata, I., Mutschmann, C., Schmitz, J., Gibson, S., Judge, K., Aruda Indig, M., Lu, B., Taufman, D., Sanfilippo, A. M., Shallenberger, W., Graminske, S., McLean, R., Hsen, R. I., d'Empaire, N., Dean, K., and O'Gorman, M.: Accurate and reproducible enumeration of T-, B-, and NK lymphocytes using the BD

FACSLyric 10-color system: A multisite clinical evaluation, PLoS ONE, 14, e0211207, https://doi.org/10.1371/journal.pone.0211207, 2019.

Paquette, A., Sousa-Silva, R., Fernandez, M., Faticov, M., Schillé, L., Bacon, E., Cameron, E., Fraysse, J., gagnon Koudji, E., Poirier, S., Rondeau-Leclaire, J., Tardif, S., Handa, T., Laforest-Lapointe, I., Puric-Mladenovic, D., and Ziter, C.: Montreal Urban Observatory: research platform to monitor urban forest ecosystems for global change adaptation and health, https://doi.org/https://doi.org/10.64898/2026.02.07.704556, 2026.

Pöhlker, C., Huffman, J. A., Förster, J.-D., and Pöschl, U.: Autofluorescence of atmospheric bioaerosols: spectral fingerprints and taxonomic trends of pollen, Atmos. Meas. Tech., 6, 3369–3392, https://doi.org/10.5194/amt-6-3369-2013, 2013.

Šaulienė, I., Šukienė, L., Daunys, G., Valiulis, G., Vaitkevičius, L., Matavulj, P., Brdar, S., Panic, M., Sikoparija, B., Clot, B., Crouzy, B., and Sofiev, M.: Automatic pollen recognition with the Rapid-E particle counter: the first-level procedure, experience and next steps, Atmos. Meas. Tech., 12, 3435–3452, https://doi.org/10.5194/amt-12-3435-2019, 2019.

Savouré, M., Bousquet, J., Jaakkola, J. J. K., Jaakkola, M. S., Jacquemin, B., and Nadif, R.: Worldwide prevalence of rhinitis in adults: A review of definitions and temporal evolution, Clinical & Translational All, 12, e12130, https://doi.org/10.1002/clt2.12130, 2022.

Sikoparija, B., Matavulj, P., Simovic, I., Radisic, P., Brdar, S., Minic, V., Tesendic, D., Kadantsev, E., Palamarchuk, J., and Sofiev, M.: Classification accuracy and compatibility across devices of a new Rapid-E+ flow cytometer, https://doi.org/10.5194/egusphere-2024-187, 2 April 2024.

Smith, E. G.: Sampling and identifying allergenic pollens and molds. An illustrated manual for physicians and lab technicians., Sampling and identifying allergenic pollens and molds. An illustrated manual for physicians and lab technicians., 1984.

Solly, F., Rigollet, L., Baseggio, L., Guy, J., Borgeot, J., Guérin, E., Debliquis, A., Drenou, B., Campos, L., Lacombe, F., and Béné, M. C.: Comparable flow cytometry data can be obtained with two types of instruments, Canto II, and Navios. A GEIL study, Cytometry A, 83, 1066–1072, https://doi.org/10.1002/cyto.a.22404, 2013.

Sousa-Silva, R., Smargiassi, A., Paquette, A., Kaiser, D., and Kneeshaw, D.: Exactly what do we know about tree pollen allergenicity?, The Lancet Respiratory Medicine, 8, e10, https://doi.org/10.1016/S2213-2600(19)30472-2, 2020.

Steckling-Muschack, N., Mertes, H., Mittermeier, I., Schutzmeier, P., Becker, J., Bergmann, K.-C., Böse-O'Reilly, S., Buters, J., Damialis, A., Heinrich, J., Kabesch, M., Nowak, D., Walser-Reichenbach, S., Weinberger, A., Zamfir, M., Herr, C., Kutzora, S., and Heinze, S.: A systematic review of threshold values of pollen concentrations for symptoms of allergy, Aerobiologia, 37, 395–424, https://doi.org/10.1007/s10453-021-09709-4, 2021.

Swanson, B., Freeman, M., Rezgui, S., and Huffman, J. A.: Pollen classification using a single particle fluorescence spectroscopy technique, Aerosol Science and Technology, 57, 112–133, https://doi.org/10.1080/02786826.2022.2142510, 2023.

Tardif, S.: Pollen Flow Cytometry Datasets and Classification Models. (v1), https://doi.org/https://doi.org/10.6084/m9.figshare.30870641, 2025.

Tummon, F., Adams-Groom, B., Antunes, C. M., Bruffaerts, N., Buters, J., Cariñanos, P., Celenk, S., Choël, M., Clot, B., Cristofori, A., Crouzy, B., Damialis, A., Fernández, A. R., González, D. F., Galán, C., Gedda, B., Gehrig, R., Gonzalez-Alonso, M., Gottardini, E., Gros-Daillon, J., Hajkova, L., O'Connor, D., Östensson, P., Oteros, J., Pauling, A., Pérez-Badia, R., Rodinkova, V., Rodríguez-Rajo, F. J., Ribeiro, H., Sauliene, I., Sikoparija, B., Skjøth, C. A., Spanu, A., Sofiev, M., Sozinova, O., Srnec, L., Visez, N., and De Weger, L. A.: The role of automatic pollen and fungal spore monitoring across major end-user domains, Aerobiologia, 40, 57–75, https://doi.org/10.1007/s10453-024-09820-2, 2024.

Wang, L. and Hoffman, R. A.: Standardization, Calibration, and Control in Flow Cytometry, CP Cytometry, 79, https://doi.org/10.1002/cpcy.14, 2017.

Zhang, G. and Abdulla, W.: Identifying Pollen Species Using Multispectral Imaging Flow Cytometry and Neural Networks, https://doi.org/10.2139/ssrn.4375939, 2023.

Zhang, Y. and Steiner, A. L.: Projected climate-driven changes in pollen emission season length and magnitude over the continental United States, Nat Commun, 13, 1234, https://doi.org/10.1038/s41467-022-28764-0, 2022.

Ziska, L. H., Makra, L., Harry, S. K., Bruffaerts, N., Hendrickx, M., Coates, F., Saarto, A., Thibaudon, M., Oliver, G., Damialis, A., Charalampopoulos, A., Vokou, D., Heiðmarsson, S., Guðjohnsen, E., Bonini, M., Oh, J.-W., Sullivan, K., Ford, L., Brooks, G. D., Myszkowska, D., Severova, E., Gehrig, R., Ramón, G. D., Beggs, P. J., Knowlton, K., and Crimmins, A. R.: Temperature-related changes in airborne allergenic pollen abundance and seasonality across the northern hemisphere: a retrospective data analysis, The Lancet Planetary Health, 3, e124–e131, https://doi.org/10.1016/S2542-5196(19)30015-4, 2019.